A&A 447, 1165–1174 (2006)
DOI: 10.1051/0004-6361:20053278
© ESO 2006

Astronomy & Astrophysics

Dielectronic recombination data for dynamic finite-density plasmas

XI. The sodium isoelectronic sequence

Z. Altun[1], A. Yumak[1], N. R. Badnell[2], S. D. Loch[3], and M. S. Pindzola[3]

[1] Department of Physics, Marmara University, Istanbul 34722, Turkey
e-mail: zikalt@superonline.com
[2] Department of Physics, University of Strathclyde, Glasgow G4 0NG, UK
[3] Department of Physics, Auburn University, Auburn, AL 36849, USA

Received 21 April 2005 / Accepted 28 June 2005

ABSTRACT

Dielectronic recombination (DR) rate coefficients for 22 sodium-like ions, between Mg^{+} and Xe^{43+}, forming magnesium-like ions have been calculated as part of the assembly of a level-resolved DR database necessary for modelling dynamic finite-density plasmas, within the generalized collisional–radiative framework. Calculations have been performed from both ground and metastable initial states, in both *LS* - and intermediate coupling, allowing for $\Delta n = 0$ and $\Delta n = 1$ core-excitations from ground and metastable levels. Partial and total DR coefficients have been calculated for Mg^{+} to Zn^{19+}, as well as Kr^{25+}, Mo^{31+}, and Xe^{43+}. Results for a selection of ions from the sequence are discussed in the paper and compared with existing theoretical and experimental results. A full set of results can be accessed from the Atomic Data and Analysis Structure (ADAS) database or from the Oak Ridge Controlled Fusion Atomic Data Center (http://www-cfadc.phy.ornl.gov/data_and_codes).

Key words. atomic data – atomic processes

1. Introduction

Dielectronic recombination (DR) is the dominant electron-ion recombination process in many astrophysical and laboratory plasmas. In this process, a free electron can collisionally excite an ion and be simultaneously captured into an autoionizing state of the recombined system. DR occurs if the resulting doubly-excited state subsequently decays radiatively below the first ionization threshold. DR rate coefficients are needed for determining both the level populations and the ionization balance of plasmas over a wide range of electron temperatures and densities and plasma timescales. Reliable DR rate coefficients are essential for the spectral diagnosis of non-equilibrium laboratory and astrophysical plasmas.

The pioneering work of Burgess (1964, 1965) resulted in a semi-empirical analytic expression for DR rate coefficients summed over all final states, for a given dipole core excitation from the initial ground state. More detailed studies of the DR of Na-like ions prior to 1998 are summarized, and data compiled in the form of fitted parameters suitable for DR rate coefficients to be used in modelling plasmas, by Shull and van Steenberg (1982), Nussbaumer & Storey (1983), Arnaud & Rothenflug (1985), Arnaud & Raymond (1992) and Mazzotta et al. (1998). These calculations were done for the ground states and often using single-configuration *LS* -coupling approximations or semi-empirical formulae or isoelectronic interpolations without considering metastable initial states. There is a critical review of many of these studies and others in Savin & Laming (2002). Since then Gu (2004) has carried out calculations of total DR rate coefficients for Na-like ions ranging from Mg to Zn within a fully-relativistic factorized distorted-wave approximation.

Developments in experimental techniques for studying DR, such as electron beam ion traps (EBITs) and heavy-ion storage rings with a merged electron-ion beam interaction region, make it possible to measure DR cross sections at high resolution, sometimes from metastable states as well as the ground. In turn, theory must take account of configuration mixing and relativistic effects and include in detail all possible levels contributing to DR. Specific measurements utilizing an electron-cooler have been made for the dielectronic recombination of Na-like ions by Linkemann et al. (1995) for Fe^{15+} and by Fogle et al. (2003a,b) for Ni^{17+}.

Recently, an international effort has been undertaken to calculate DR rate coefficients for K-, L- and M-shell ions from both the ground and metastable states. The details of the methodology used in this effort to set up the total and final-state level-resolved intermediate coupling DR database

Article published by EDP Sciences and available at http://www.edpsciences.org/aa or http://dx.doi.org/10.1051/0004-6361:20053278

necessary for the spectroscopic modelling of dynamic finite-density plasmas, where the coronal approximation is not valid, has been described by Badnell et al. (2003). The final-state, level-resolved DR rate coefficients are important for the collisional-radiative modelling of dense plasmas. The DR rate coefficients obtained from metastable states are important for modelling dynamic plasmas where there exist excited states with significant populations that are not in quasi-static equilibrium with the ground state. To this end, a number of calculations have been performed so far, in both *LS* - and intermediate coupling, for DR rate coefficients from both the ground and metastable initial states of the following isoelectronic sequences of target ions: lithium (Colgan et al. 2004), beryllium (Colgan et al. 2003), boron (Altun et al. 2004), carbon (Zatsarinny et al. 2004a), nitrogen (Mitnik et al. 2004), oxygen (Zatsarinny et al. 2003 and neon (Zatsarinny et al. 2004b).

As compared to the wealth of information concerning DR data for K-shell and L-shell ions in the literature, one can only find a few studies in the literature concerning DR for M-shell ions. Netzer (2004) and Kraemer et al. (2004) examined the effects of low-temperature, or $\Delta n = 0$ core excitation, DR on the ionization balance of Fe M-shell ions in photoionized plasmas and they demonstrated the critical need for reliable DR rate coefficients for Fe M-shell ions. This is necessary in order to resolve the transition array of inner-shell 2–3 lines seen in high resolution X-ray spectra of Seyfert Galaxies observed with XMM-Newton and Chandra. Netzer (2004) has concluded that without reliable Fe M-shell DR data, it is not possible to model photoionized plasmas where there are strong overlaps from 2–3 inner shell transition lines of FeI–FeXVI superimposed on the spectra corresponding to H-like, He-like lines and inner shell lines of silicon, sulphur and iron.

The effect of weak external electric fields on the high Rydberg states which frequently dominate the dielectronic recombination process was discussed by Burgess & Summers (1969). The effect of the plasma microfield on dielectronic recombination was studied by Jacobs et al. (1976). The effects of external electric fields on dielectronic recombination are found to be quite significant by Griffin et al. (1986) in their studies of Na-like ions P^{4+}, S^{5+}, Cl^{6+} and by Griffin & Pindzola (1987) in their studies of Fe^{15+}. Recent experimental (Bartsch et al. 1997, 1999; Böhm et al. 2001, 2002; Schippers et al. 2000; Gwinner et al. 2000), and theoretical studies (Robicheaux & Pindzola 1997; Robicheaux et al. 1998; Griffin et al. 1998; Mitnik et al. 1999) have shown the importance of the effects of crossed external electric and magnetic fields. We expect that low charge Na-like ions will be more sensitive to the external fields, as is the case for Li-like ions (Badnell et al. 1993). It was shown that the inclusion of electric field effects gave very good agreement between the intermediate coupling calculations by Griffin et al. (1989) and measurements by Andersen et al. (1990) of dielectronic recombination for C^{3+} and O^{5+}, but (crossed) magnetic fields were not considered. As explained by Badnell et al. (1993, 2003), field-free data is the most suitable starting point for plasma modelling. Subsequently, allowance for *l*-changing collisions within the collisional-radiative population equations represents the dynamic part of the plasma microfield.

In this paper, we describe calculations and present results for the DR of sodium-like ions using a multiconfiguration intermediate coupling Breit-Pauli (MCBP) approximation. In calculating "M-shell" DR for Na-like ions we have considered both $\Delta n = 0$ and $\Delta n = 1$ core excitations involving 2p and 3s, 3p subshells during the capture of the colliding electron. We note the importance of $2 \rightarrow 3$ $\Delta n = 1$ core excitations at high temperatures for high-*Z* ions in discussing the results. DR associated with $\Delta n = 0$ core excitations occurs at much lower temperatures and is the dominant recombination process in photoionized plasmas. We also compute and compare *LS* -coupling results because as we progress into the M-shell it becomes increasingly demanding to carry out Breit-Pauli calculations. *LS* -coupling calculations are an order of magnitude less demanding than Breit-Pauli and so they enable us to investigate the rôle of various configurations and, ultimately, may be all that it is tractable to calculate.

The main goal of this work is to calculate multi-configuration intermediate coupling M-shell DR rate coefficients from the ground plus metastable initial states of an ion to all possible final states, resolved to a degree appropriate for generalized collisional-radiative modelling. When the timescale of change in electron temperature and electron densities of a plasma is comparable with the lifetime of the metastable populations of its constituent ions then these populations may no longer be assumed to be in quasi-static equilibrium with the ground state. For these situations accurate population modelling DR from metastable states must be considered on an equal footing with the ground states. As was the case for Li-like ions, it is sometimes necessary to treat (in this instance) the 3p state as metastable. Final-state level-resolved dielectronic recombination rate coefficients are important for the collisional-radiative modelling of finite-density plasmas where stepwise ionization can significantly reduce the effective recombination rate coefficient compared with its low-density limit.

Calculations have been carried-out over a wide range of electron temperatures, $Z^2(10-10^7)$ K where *Z* is the electron target ion charge, for 22 Na-like ions from Mg to Xe. Results are presented in both *LS* - and intermediate coupling approximations. Our intermediate coupling MCBP results are found to be in good agreement with other existing measurements and calculations over electron temperatures ranging from $\sim Z^2(10^3-10^7)$ K. In Sect. 2 we give a brief description of the theory used, in Sect. 3 we compare our velocity-averaged dielectronic recombination cross sections with the measurements made at storage rings utilizing electron-coolers, and in Sect. 4 we present dielectronic recombination rate coefficients for the sodium isoelectronic sequence and compare them with the results of other workers for selected ions. We conclude with a brief summary.

2. Theory

The theoretical details of our calculations have already been described (Badnell et al. 2003). Here we outline only the main points. The AUTOSTRUCTURE code (Badnell 1986, 1997) was used to calculate energy levels, radiative and

autoionization rates in the LS- and intermediate coupling (MCBP) approximations using non-relativistic (up to Zn) and semi-relativistic (from Zn) radial functions. The autoionization rates are calculated in the isolated resonance approximation using distorted waves. This enables the generation of final-state level-resolved and total dielectronic recombination rate coefficients in the independent processes approximation, i.e. we neglect interference between the radiative recombination and the dielectronic recombination processes. Although this has been found to be only a very small effect for the total rate (Pindzola et al. 1992), more recent studies of partial recombination cross sections for Li-like fluorine F^{6+} (Mitnik et al. 1999) predict some interference between these processes for weak partial cross sections.

The dielectronic capture process from the ground state of Na-like ions can be represented for $\Delta n = 0$ core-excitations by

$$\begin{aligned} 1s^2 2s^2 2p^6 3s(^2S_{1/2}) + e^- &\rightarrow 1s^2 2s^2 2p^6 3p(^2P_J) nl, \\ &\rightarrow 1s^2 2s^2 2p^6 3d(^2D_J) nl, \end{aligned} \quad (1)$$

and since the first excited configuration can be significantly populated through collisions from the ground level, we also consider

$$\begin{aligned} 1s^2 2s^2 2p^6 3p(^2P_J) + e^- &\rightarrow 1s^2 2s^2 2p^6 3p(^2P_{J'}) nl, \\ &\rightarrow 1s^2 2s^2 2p^6 3d(^2D_J) nl. \end{aligned}$$

In this case ($\Delta n = 0$), l and n values were included up to 15 and 25 respectively, and a quantum-defect theory approximation for high-level values of n up to 1000 were used (Badnell et al. 2003). All possible stabilizing radiative transitions were accounted for.

The dielectronic capture process for $\Delta n = 1$ core-excitations can be written as

$$\begin{aligned} 1s^2 2s^2 2p^6 3s(^2S_{1/2}) + e^- &\rightarrow 1s^2 2s^2 2p^6 4lnl' \\ &\rightarrow 1s^2 2s^2 2p^5 3l3l' n'' l'' \\ 1s^2 2s^2 2p^6 3p(^2P_J) + e^- &\rightarrow 1s^2 2s^2 2p^6 4lnl' \\ &\rightarrow 1s^2 2s^2 2p^5 3l3l' n'' l''. \end{aligned} \quad (2)$$

In the case of promotions from $n = 2$ we only include those from the 2p sub-shell. Test calculations show that the contribution to the total DR rate coefficient from 2s promotions is ~1%. For $\Delta n = 1$ core excitations, values of l' up to $l' = 5$ and 7 were included for $2 \rightarrow 3$ and $3 \rightarrow 4$ core excitations, respectively, while values of n up to $n = 25$ were included in both cases. Again an approximation for the high-level values of n was used up to $n = 1000$.

The dielectronic recombination rate coefficient from an initial metastable state ν to a final-state i is given by

$$\alpha_{i\nu} = \left(\frac{4\pi a_0^2 I_{\rm H}}{k_{\rm B} T_{\rm e}}\right)^{3/2} \sum_j \frac{\omega_j}{2\omega_\nu} {\rm e}^{-E_{\rm c}/k_{\rm B}T_{\rm e}} \times \frac{\sum_l A^{\rm a}_{j\rightarrow\nu,E_{\rm c}l} A^{\rm r}_{j\rightarrow i}}{\sum_h A^{\rm r}_{j\rightarrow h} + \sum_{m,l} A^{\rm a}_{j\rightarrow m,E_{\rm c}l}}, \quad (3)$$

where ω_j is the statistical weight of the $(N+1)$-electron doubly-excited resonance state j, ω_ν is the statistical weight of the N electron target state and the autoionization ($A^{\rm a}$) and radiative ($A^{\rm r}$) rates are in inverse seconds. Here, $E_{\rm c}$ is the energy of the continuum electron of angular momentum l, which is fixed by the position of the resonances, and $I_{\rm H}$ is the ionization potential energy of the hydrogen atom, $k_{\rm B}$ is the Boltzmann constant, $T_{\rm e}$ is the electron temperature and $(4\pi a_0^2)^{3/2} = 6.6011 \times 10^{-24}$ cm^3. Calculations were carried out within the independent processes and isolated resonance approximations using the AUTOSTRUCTURE computer code which is implemented within the ADAS suite of programs as ADAS701. For $\Delta n = 0$ core-excitations, the resonance energies are empirically adjusted so that the series limits match the $3 \rightarrow 3$ core-excitation energies obtained from the NIST evaluated database (`http://physics.nist.gov/`). Accurate resonance energies are particularly important for the calculations of low-temperature dielectronic recombination rate coefficients. Separate calculations are done for the different core-excitations ($\Delta n = 0$ and $\Delta n = 1$). Finally, LS- and intermediate coupling dielectronic recombination rate coefficients for different core-excitations were saved under common file names to be added to the existing Atomic Data and Analysis Structure (ADAS) database (Summers 2003).

3. Comparisons with experiments

In Fig. 1 we first compare our MCBP intermediate coupling velocity-averaged dielectronic recombination cross sections for Fe^{15+} forming Fe^{14+} via $3 \rightarrow 3$ ($\Delta n = 0$) core-excitations with measurements carried out using the heavy-ion Test Storage Ring at the Max-Planck-Institute for Nuclear Physics in Heidelberg, Germany by Linkemann et al. (1995). To compare with experiments, we have used the experimental velocity spread of Linkemann et al. (1995) associated with the relative motion between the ions and the electrons, corresponding to temperatures $k_{\rm B}T_\perp = 15$ meV perpendicular to the confining magnetic field and $k_{\rm B}T_\parallel = 0.15$ meV parallel to the magnetic field, in the convolution of our DR cross sections. To account for field ionization effects we also eliminated all resonances with $n \geq 87$, which is the experimental cutoff estimated by Linkemann et al. (1995).

DR resonances in the region below the $e^- + 3s \rightarrow 3p_{3/2} nl$ series limit at approximately 36.6 eV are predominantly due to capture to $3p_j nl_j$ and $3d_j nl_j$. The lowest resonances associated with the formation of the $3p_{3/2}10s$ doubly excited levels are located just above threshold between 1.057 eV and 3.40 eV. Resonances corresponding to $3p_{3/2}11s$ doubly excited levels are distributed between 6.70 eV and 9.30 eV. Analysis has shown strong superposition amongst resonances associated with $3p_{1/2,3/2} nl_j$, $n \geq 10$. There are also strong superpositions between $3p_j nl_j, n \geq 10$ and $3d_j nl_j, n \geq 7$ resonances above 13.79 eV. There is also superposition between ($\Delta n = 0$) resonances and ($\Delta n = 1$) from the autoionization of $1s^2 2s^2 2p^6 4l4l'$ configurations at around 31.6 eV.

Overall, our theoretical results and the experimental results of Linkemann et al. (1995) are in good agreement. The minor differences that exist between theory and experiment arise due to slight differences in the position of resonances between theory and experiment. The shift is still present for high Rydberg

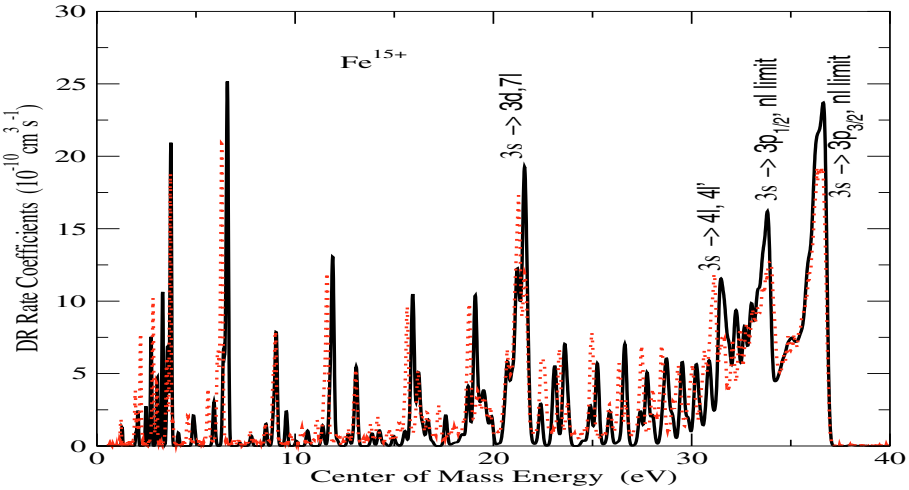

Fig. 1. Velocity-averaged dielectronic recombination cross sections for Fe^{15+}, as a function of center-of-mass collision energy in the range 0 to 40 eV. The resonances in this range are mostly associated with $n = 3 \rightarrow 3$ ($\Delta n = 0$) core-excitations. The solid line denotes our intermediate coupling MCBP results and the dotted line denotes the experimental results of Linkemann et al. (1995). Our DR cross sections (×velocity) have been convoluted with the experimental energy spread of Linkemann et al. (1995) corresponding to temperatures $k_B T_\perp$ = 15 meV and $k_B T_\parallel$ = 0.15 meV.

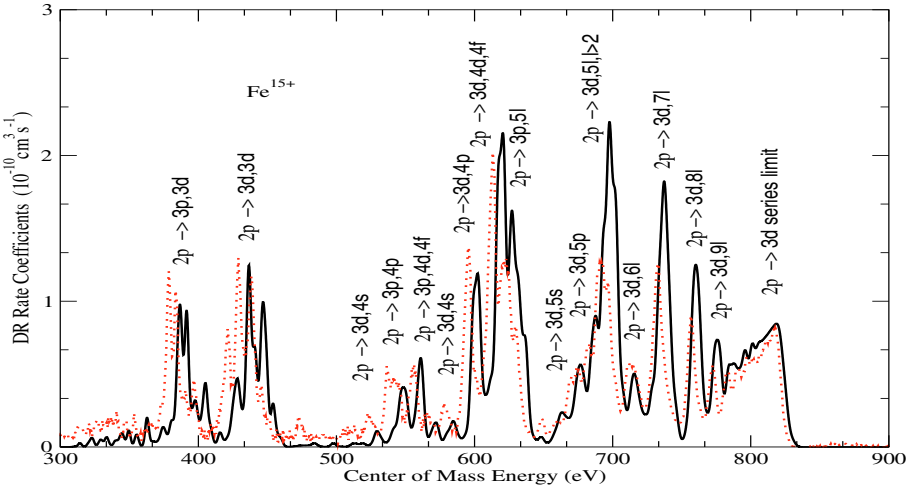

Fig. 2. Velocity-averaged dielectronic recombination cross sections for Fe^{15+}, as a function of the center-of-mass collision energy in the range 300 to 900 eV. The resonances in this range are associated with $n = 2 \rightarrow 3$ ($\Delta n = 1$) core-excitations. The solid line denotes our MCBP intermediate coupling results and the dotted line denotes the experimental results of Linkemann et al. (1995). Our DR cross sections (× velocity) have been convoluted with the experimental energy spread of Linkemann et al. (1995), corresponding to temperatures $k_B T_\perp$ = 15 meV and $k_B T_\parallel$=0.15 meV.

resonances and is unaccounted for by the small difference between the calculated and observed target energies. We do not see similar shifts in comparisons with experiments for other ions. Thus, it would appear to be an experimental artifact. Figure 1 shows that our intermediate coupling MCBP calculations reproduce all of the main features well. The agreement between theory and experiment is even good for the low-lying resonances just above threshold, where the results are quite sensitive to small energy differences in resonance positions.

In Fig. 2 we compare our MCBP intermediate coupling velocity-averaged dielectronic recombination cross sections for Fe^{15+} as a function of electron temperature with the experimental measurements by Linkemann et al. (1995), in an energy range between 300 to 900 eV. As can be seen, there is no practical difference between our intermediate coupling results and the measurements, apart from a somewhat puzzling shift in energy. There are no features that can be abscribed to 2s → 3p promotions. Resonances seen in Fig. 2 are associated with the formation of doubly-excited bound states corresponding to the $\Delta n = 1$ core excitations from the 2p and 3s sub-shells. Resonances in Fig. 2 coming from the autoionization of the first 11 levels of the $2p^5 3s^2 3p$ configuration are distributed between 283.13 eV and 299.99 eV and the one with the $^1P_0$ multiplet located at 314.28 eV is intermixed with the resonances associated with the $2p^5 3s 3p^2$ configuration. Resonances corresponding to the $2p^5 3s 3p^2$ configuration are distributed over energies ranging from 309.21 eV to 354.72 eV, of which higher lying members are intermixed with the resonances of the $2p^5 3s 3d$

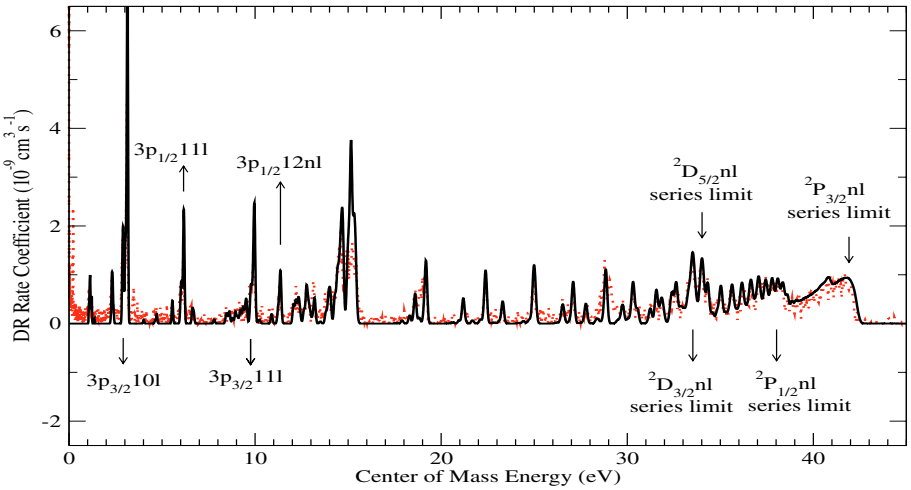

Fig. 3. Velocity-averaged dielectronic recombination cross sections for Ni^{17+}, as a function of center-of-mass collision energy in the range 0 to 45 eV. The resonances in this range are associated with 3s → 3p, d ($\Delta n = 0$) core-excitations. The solid curve represents our MCBP intermediate coupling results. The experimental results of Fogle et al. (2003b) are represented in dotted line. Our DR cross sections (×velocity) have been convoluted with the experimental energy spread of Fogle et al. (2003), corresponding to temperatures $k_B T_\perp = 1$ meV and $k_B T_\parallel = 0.1$ meV.

configuration. Resonances corresponding to the $2p^5 3s3p3d$ and $2p^5 3s3p^3$ configurations are intermixed and distributed over energies ranging from 356.04 eV to 406.04 eV. Some higher lying resonance levels of the $2p^5 3s3p3d$ configuration are intermixed with the resonances corresponding to the $2p^5 3p^2 3d$ and $2p^5 3s3d^2$ configurations at higher energies. Resonances between 395.72 eV and 442.38 eV result from the intermixing of the resonances associated with the $2p^5 3s3d^2$ and $2p^5 3p^2 3d$ configurations and there are also a few resonances in this region eminating from the $2p^5 3s3p3d$ configuration. We have compared our calculations done using the Slater-type orbital potential with the calculations done using the Thomas-Fermi potential and we have not seen any significant changes in the energy positions of the resonances at around 400 eV as a result of varying the atomic structure. The region between 443.24 eV and 542.48 eV is dominated by resonances corresponding to the configurations $2p^5 3s3p3d$ and $2p^5 3d^3$. The lower part of this region has strong intermixing from the resonances associated with the $2p^5 3s3d^2$ configuration. Resonances in the energy region between 500 to 815 eV correspond to the $2p \rightarrow 3lnl$ with $n \geq 4$ excitations.

In Fig. 3 we compare our MCBP intermediate coupling velocity-averaged dielectronic recombination cross sections for Ni^{17+} with the experimental results of Fogle et al. (2003b) as a function of the center-of-mass collision energy range 0 to 43 eV. This energy range covers all $\Delta n = 0$ resonances associated with the $3p_j nl_j$ ($n \geq 10$) and $3d_j nl_j$ ($n \geq 7$) doubly excited states. Doubly excited states $3p_{1/2}10l_j$ lie just below the ionization limit, i.e. they are true bound states. The lowest resonances just above the threshold in Fig. 3 thus correspond to $3p_{3/2}10l_j$ autoionizing states. The lowest resonance of the form $3p_{1/2}11l_j$ is located at 6.057 eV, and has the orbital angular momentum $l = 0$. Further resonances are labelled in Fig. 3. The results of our MCBP calculations (represented by solid line in Fig. 3 agree well with the experiment. Near the Rydberg limits it is necessary to model the time-of-flight of recombined states from the cooler to the charge-state analyzer since some recombined states have time to decay to lower lying levels and so survive field ionization by the analyzer, which they would not otherwise do – see Fogle et al. (2003b) for a detailed discussion of the problem. We obtained the best agreement with a time-of-flight of 10ns.

The agreement between theory and experiment for Fe^{15+} and Ni^{17+} benchmarks our systematic study of the dielectronic recombination of sodium-like ions, particularly for the more highly charged ions. For lower charge ions our main point of assessment is the comparison with previous theoretical total Maxwellian rate coefficients, which we explore in the next section.

4. Results for rate coefficients

Numerical results, obtained in both *LS*- and intermediate coupling and for both $\Delta n = 0$ and $\Delta n = 1$ core excitations, are available on the web (`http://www-cfadc.phy.ornl.gov/data_and_codes`) in the ADAS *adf09* format (Summers 2003). They provide final-state resolved dielectronic recombination rate coefficients from both the ground and metastable initial states into final *LS* terms or *LSJ* levels in a manner useful to fusion and astrophysical modellers. We have also used the formula

$$\alpha = \frac{1}{T^{3/2}} \sum_{i=1}^{n} c_i e^{-E_i/T}, \qquad (4)$$

where n ranges from 3 to 7 depending on the ion, to fit all of our intermediate coupling total DR rate coefficients so as to facilitate the use of our data by others. In this equation, T and E_i have units of Kelvin and the rate coefficients α have units of cm^3 s^{-1}. Our fits are accurate to better than ≈5% for all ions in the temperature range $Z^2(10-10^7)$ K, where Z is the residual charge of the initial ion. In fact, this 5% applies only over limited energy ranges where the DR has a local minimum. The accuracy is typically better than 1% over the broad

Table 1. Fitting coefficients c_i and E_i for Eq. (4), for ions in the sodium isoelectronic sequence forming magnesium like systems. All coefficients refer to our intermediate coupling calculations obtained on using non-relativistic (up to Zn) and semi-relativistic (from Zn) radial functions. $X(Y)$ means $X \times 10^Y$.

Ion	c_1	c_2	c_3	c_4	c_5	c_6	c_7
Mg^{1+}	3.871(−8)	4.732(−7)	1.599(−3)	2.628(−5)	···	···	···
Al^{2+}	1.629(−6)	3.584(−6)	1.244(−5)	4.155(−3)	2.904(−4)	···	···
Si^{3+}	3.819(−6)	2.421(−5)	2.283(−4)	8.604(−3)	2.617(−3)	···	···
P^{4+}	2.722(−7)	7.538(−5)	1.466(−4)	1.402(−2)	5.283(−4)	3.280(−3)	···
S^{5+}	2.816(−6)	3.172(−5)	1.832(−4)	4.360(−3)	1.618(−2)	7.707(−3)	···
Cl^{6+}	2.041(−5)	2.386(−4)	8.413(−4)	2.724(−2)	8.375(−3)	1.595(−2)	···
Ar^{7+}	1.016(−4)	7.473(−4)	3.394(−2)	2.398(−3)	2.530(−2)	···	···
K^{8+}	1.030(−6)	3.755(−4)	1.354(−3)	4.108(−2)	4.373(−3)	4.094(−2)	···
Ca^{9+}	6.508(−5)	8.795(−4)	6.576(−3)	4.780(−2)	5.167(−2)	1.859(−2)	···
Sc^{10+}	1.120(−4)	1.532(−3)	2.899(−3)	5.815(−2)	9.603(−3)	1.027(−1)	6.511(−4)
Ti^{11+}	1.264(−4)	8.031(−4)	4.274(−3)	6.761(−2)	1.252(−2)	1.583(−1)	1.625(−3)
V^{12+}	3.510(−5)	1.137(−3)	8.161(−3)	7.833(−2)	2.057(−2)	5.152(−2)	1.922(−1)
Cr^{13+}	1.437(−4)	2.295(−3)	1.174(−2)	8.706(−2)	3.242(−2)	1.170(−1)	2.616(−1)
Mn^{14+}	1.050(−3)	5.850(−3)	1.115(−2)	9.993(−2)	6.156(−2)	5.521(−1)	···
Fe^{15+}	7.676(−4)	5.587(−3)	1.152(−1)	4.929(−2)	7.274(−1)	7.347(−3)	···
Co^{16+}	1.243(−3)	8.226(−3)	1.223(−1)	4.428(−2)	3.794(−1)	5.032(−1)	···
Ni^{17+}	3.419(−4)	4.806(−3)	3.420(−2)	1.305(−1)	1.145(−1)	9.603(−1)	1.076(−2)
Cu^{18+}	3.268(−3)	8.279(−3)	4.809(−2)	1.384(−1)	2.247(−1)	1.030(+0)	···
Zn^{19+}	8.941(−4)	1.879(−2)	4.694(−2)	1.560(−1)	2.083(−1)	1.258(+0)	8.934(−3)
Kr^{25+}	1.658(−3)	5.980(−2)	1.403(−1)	1.958(−1)	5.874(−1)	2.472(+0)	1.321(−2)
Mo^{31+}	1.256(−2)	4.977(−2)	3.037(−1)	2.477(−1)	1.007(+0)	3.570(+0)	2.740(−2)
Xe^{43+}	3.876(−2)	1.393(−1)	8.111(−1)	3.756(−1)	3.164(+0)	5.596(+0)	···
	E_1	E_2	E_3	E_4	E_5	E_6	E_7
Mg^{1+}	8.415(+3)	1.682(+4)	5.0000(+4)	2.759(+5)	···	···	···
Al^{2+}	3.809(+3)	5.120(+3)	2.166(+4)	7.635(+4)	8.477(+5)	···	···
Si^{3+}	3.802(+3)	1.280(+4)	5.953(+4)	1.026(+5)	1.154(+6)	···	···
P^{4+}	3.732(+3)	2.407(+4)	5.213(+4)	1.247(+5)	8.053(+5)	1.513(+6)	···
S^{5+}	7.590(+3)	1.558(+4)	4.013(+4)	1.156(+5)	1.601(+5)	1.839(+6)	···
Cl^{6+}	1.279(+4)	2.238(+4)	6.587(+4)	1.786(+5)	1.782(+6)	2.767(+6)	···
Ar^{7+}	1.513(+4)	4.784(+4)	1.926(+5)	6.904(+5)	2.715(+6)	···	···
K^{8+}	2.685(+3)	1.684(+4)	5.729(+4)	2.141(+5)	8.556(+5)	3.198(+6)	···
Ca^{9+}	3.711(+3)	4.421(+4)	1.189(+5)	2.603(+5)	3.099(+6)	5.016(+6)	···
Sc^{10+}	2.655(+3)	1.861(+4)	5.316(+4)	2.604(+5)	1.186(+6)	4.210(+6)	1.896(+7)
Ti^{11+}	4.550(+3)	1.434(+4)	9.989(+4)	2.879(+5)	1.331(+6)	4.770(+6)	3.999(+7)
V^{12+}	1.209(+4)	4.097(+4)	1.163(+5)	3.182(+5)	1.659(+6)	4.589(+6)	5.804(+6)
Cr^{13+}	8.994(+3)	2.734(+4)	1.091(+5)	3.430(+5)	1.913(+6)	5.724(+6)	6.593(+6)
Mn^{14+}	9.125(+3)	2.730(+4)	1.065(+5)	3.718(+5)	2.640(+6)	7.225(+6)	···
Fe^{15+}	2.935(+4)	8.158(+4)	3.591(+5)	1.735(+6)	7.545(+6)	4.634(+7)	···
Co^{16+}	1.105(+4)	8.003(+4)	3.613(+5)	1.193(+6)	6.235(+6)	9.861(+6)	···
Ni^{17+}	1.531(+4)	4.515(+4)	1.905(+5)	4.703(+5)	3.115(+6)	9.270(+6)	3.490(+7)
Cu^{18+}	1.353(+4)	6.265(+4)	2.089(+5)	5.423(+5)	4.439(+6)	1.059(+7)	···
Zn^{19+}	8.004(+3)	5.730(+4)	2.268(+5)	5.609(+5)	4.164(+6)	1.106(+7)	3.900(+7)
Kr^{25+}	3.164(+4)	1.120(+5)	4.055(+5)	8.992(+5)	6.219(+6)	1.660(+7)	2.308(+8)
Mo^{31+}	3.225(+4)	1.285(+5)	5.876(+5)	1.354(+6)	7.962(+6)	2.273(+7)	4.910(+8)
Xe^{43+}	6.311(+4)	2.635(+5)	1.087(+6)	3.678(+6)	1.693(+7)	4.238(+7)	···

range of temperatures where DR dominates in both collision dominated and photoionized plasmas. In Table 1 we present fitting coefficients c_i and E_i for each member of the sodium isoelectronic sequence considered. These fitting coefficients have been obtained for the sum of the dielectronic recombination rate coefficients calculated separately for $\Delta n = 0$ and $\Delta n = 1$ core-excitations.

An important aspect of this work is the archiving of final-state level-resolved partial DR rate coefficients. As an example of this we present partial rate coefficients for Fe^{15+} in Table 2. Of course, there are hundreds of final state levels for this ion but we just present the first 24 to emphasize the detailed information that can be obtained from the MCBP calculation for DR of highly complex ions such as Fe^{15+}. The rest of the final state level resolved partial rate coefficients can easily be accessed from the ORNL archive.

In Fig. 4 we compare our MCBP intermediate coupling total dielectronic recombination rate coefficients for Fe^{15+} as a

Table 2. Final state level-resolved rate coefficients from the $1s^2 2s^2 2p^6 3s\ ^2S_{1/2}$ ground state of Fe^{15+} to the lowest 24 levels of Fe^{14+}. $X(Y)$ means $X \times 10^Y$.

T(K)	$3s^2(^1S_0)$	$3s3p(^3P_0)$	$3s3p(^3P_1)$	$3s3p(^3P_2)$	$3s3p(^1P_1)$	$3p^2(^3P_0)$	$3p^2(^1D_0)$	$3p^2(^3P_1)$
2.25(+3)	2.74(−16)	1.31(−15)	2.63(−15)	8.07(−19)	8.14(−16)	1.30(−14)	3.19(−14)	2.54(−14)
4.50(+3)	2.79(−15)	8.74(−14)	1.85(−13)	6.03(−16)	5.63(−14)	1.37(−13)	3.34(−13)	2.60(−13)
1.13(+4)	1.00(−14)	5.18(−13)	1.15(−12)	1.78(−13)	4.07(−13)	5.66(−13)	1.38(−12)	1.10(−12)
2.25(+4)	1.60(−14)	5.45(−13)	1.31(−12)	7.16(−13)	6.37(−13)	7.94(−13)	2.13(−12)	1.68(−12)
4.50(+4)	1.73(−14)	3.88(−13)	1.01(−12)	9.95(−13)	6.49(−13)	7.16(−13)	2.16(−12)	1.66(−12)
1.13(+5)	1.33(−14)	2.16(−13)	6.08(−13)	8.28(−13)	4.79(−13)	4.77(−13)	1.60(−12)	1.19(−12)
2.25(+5)	8.54(−15)	1.25(−13)	3.61(−13)	5.44(−13)	3.06(−13)	2.91(−13)	1.01(−12)	7.43(−13)
4.50(+5)	4.39(−15)	6.09(−14)	1.79(−13)	2.84(−13)	1.58(−13)	1.46(−13)	5.15(−13)	3.77(−13)
1.13(+6)	1.43(−15)	1.93(−14)	5.73(−14)	9.36(−14)	5.18(−14)	4.71(−14)	1.67(−13)	1.22(−13)
2.25(+6)	5.54(−16)	7.39(−15)	2.20(−14)	3.63(−14)	2.01(−14)	1.81(−14)	6.42(−14)	4.72(−14)
4.50(+6)	2.05(−16)	2.72(−15)	8.13(−15)	1.35(−14)	7.44(−15)	6.70(−15)	2.37(−14)	1.74(−14)
1.13(+7)	5.33(−17)	7.07(−16)	2.11(−15)	3.51(−15)	1.94(−15)	1.74(−15)	6.17(−15)	4.53(−15)
2.25(+7)	1.90(−17)	2.52(−16)	7.53(−16)	1.25(−15)	6.92(−16)	6.21(−16)	2.20(−15)	1.62(−15)
4.50(+7)	6.76(−18)	8.94(−17)	2.67(−16)	4.45(−16)	2.46(−16)	2.20(−16)	7.82(−16)	5.74(−16)
1.13(+8)	1.71(−18)	2.27(−17)	6.78(−17)	1.13(−16)	6.23(−17)	5.59(−17)	1.98(−16)	1.46(−16)
2.25(+8)	6.06(−19)	8.03(−18)	2.40(−17)	4.00(−17)	2.21(−17)	1.98(−17)	7.02(−17)	5.15(−17)
4.50(+8)	2.15(−19)	2.84(−18)	8.49(−18)	1.41(−17)	7.80(−18)	7.00(−18)	2.48(−17)	1.82(−17)

T(K)	$3p^2(^3P_2)$	$3p^2(^1S_0)$	$3s3d\ (^3D_1)$	$3s3d(^3D_2)$	$3s3d(^3D_3)$	$3s3d(^1D_2)$	$3p3d(^3F_2)$	$3p3d(^3F_3)$
2.25(+3)	2.49(−15)	2.46(−15)	1.50(−18)	7.64(−18)	1.42(−21)	3.75(−15)	3.55(−16)	1.82(−16)
4.50(+3)	2.69(−14)	2.60(−14)	1.51(−17)	7.97(−17)	1.36(−18)	3.95(−14)	2.93(−14)	1.95(−14)
1.13(+4)	2.69(−13)	1.38(−13)	5.82(−17)	3.23(−16)	4.63(−17)	1.80(−13)	6.13(−13)	4.91(−13)
2.25(+4)	9.01(−13)	3.16(−13)	2.31(−15)	4.22(−15)	4.31(−15)	3.30(−13)	1.28(−12)	1.20(−12)
4.50(+4)	1.35(−12)	4.19(−13)	5.25(−14)	9.20(−14)	1.09(−13)	4.40(−13)	1.41(−12)	1.57(−12)
1.13(+5)	1.21(−12)	3.63(−13)	1.83(−13)	3.27(−13)	4.03(−13)	5.29(−13)	1.29(−12)	1.69(−12)
2.25(+5)	8.06(−13)	2.43(−13)	1.74(−13)	3.12(−13)	3.88(−13)	4.14(−13)	9.38(−13)	1.34(−12)
4.50(+5)	4.21(−13)	1.28(−13)	1.06(−13)	1.92(−13)	2.38(−13)	2.36(−13)	5.25(−13)	8.22(−13)
1.13(+6)	1.38(−13)	4.21(−14)	3.84(−14)	6.94(−14)	8.59(−14)	8.19(−14)	1.84(−13)	3.13(−13)
2.25(+6)	5.37(−14)	1.63(−14)	1.54(−14)	2.79(−14)	3.44(−14)	3.24(−14)	7.33(−14)	1.29(−13)
4.50(+6)	1.99(−14)	6.06(−15)	5.79(−15)	1.05(−14)	1.29(−14)	1.21(−14)	2.76(−14)	4.95(−14)
1.13(+7)	5.18(−15)	1.58(−15)	1.52(−15)	2.76(−15)	3.40(−15)	3.18(−15)	7.25(−15)	1.32(−14)
2.25(+7)	1.85(−15)	5.64(−16)	5.46(−16)	9.90(−16)	1.22(−15)	1.14(−15)	2.60(−15)	4.74(−15)
4.50(+7)	6.56(−16)	2.00(−16)	1.94(−16)	3.52(−16)	4.34(−16)	4.05(−16)	9.24(−16)	1.69(−15)
1.13(+8)	1.67(−16)	5.08(−17)	4.93(−17)	8.95(−17)	1.10(−16)	1.03(−16)	2.35(−16)	4.29(−16)
2.25(+8)	5.89(−17)	1.80(−17)	1.75(−17)	3.17(−17)	3.90(−17)	3.64(−17)	8.31(−17)	1.52(−16)
4.50(+8)	2.08(−17)	6.36(−18)	6.18(−18)	1.12(−17)	1.38(−17)	1.29(−17)	2.94(−17)	5.38(−17)

T(K)	$3p3d(^1D_2)$	$3p3d(^3F_4)$	$3p3d(^3D_1)$	$3p3d(^3P_2)$	$3p3d(^3D_3)$	$3p3d(^3P_0)$	$3p3d(^3P_1)$	$3p3d(^3D_2)$
2.25(+3)	8.36(−17)	8.88(−22)	1.20(−16)	1.69(−16)	6.34(−17)	1.86(−18)	2.78(−18)	9.69(−18)
4.50(+3)	8.61(−15)	6.25(−17)	1.19(−14)	1.77(−14)	7.00(−15)	1.33(−16)	2.14(−16)	8.47(−16)
1.13(+4)	2.32(−13)	7.72(−14)	2.88(−13)	4.36(−13)	2.23(−13)	8.79(−15)	2.60(−14)	5.90(−14)
2.25(+4)	6.63(−13)	6.18(−13)	6.50(−13)	1.00(−12)	7.65(−13)	6.71(−14)	2.04(−13)	3.71(−13)
4.50(+4)	9.89(−13)	1.37(−12)	7.70(−13)	1.21(−12)	1.27(−12)	1.51(−13)	4.57(−13)	7.85(−13)
1.13(+5)	1.15(−12)	1.93(−12)	7.37(−13)	1.20(−12)	1.54(−12)	2.08(−13)	6.27(−13)	1.07(−12)
2.25(+5)	8.97(−13)	1.63(−12)	5.32(−13)	8.99(−13)	1.24(−12)	1.63(−13)	4.93(−13)	8.61(−13)
4.50(+5)	5.16(−13)	1.01(−12)	2.91(−13)	5.06(−13)	7.40(−13)	9.15(−14)	2.78(−13)	5.02(−13)
1.13(+6)	1.82(−13)	3.83(−13)	9.92(−14)	1.76(−13)	2.74(−13)	3.15(−14)	9.63(−14)	1.79(−13)
2.25(+6)	7.27(−14)	1.57(−13)	3.90(−14)	6.99(−14)	1.11(−13)	1.24(−14)	3.81(−14)	7.15(−14)
4.50(+6)	2.74(−14)	6.01(−14)	1.46(−14)	2.62(−14)	4.24(−14)	4.65(−15)	1.43(−14)	2.69(−14)
1.13(+7)	7.19(−15)	1.59(−14)	3.82(−15)	6.88(−15)	1.12(−14)	1.22(−15)	3.74(−15)	7.09(−15)
2.25(+7)	2.57(−15)	5.73(−15)	1.36(−15)	2.46(−15)	4.03(−15)	4.35(−16)	1.34(−15)	2.54(−15)
4.50(+7)	9.16(−16)	2.04(−15)	4.85(−16)	8.77(−16)	1.44(−15)	1.55(−16)	4.75(−16)	9.03(−16)
1.13(+8)	2.33(−16)	5.19(−16)	1.23(−16)	2.23(−16)	3.65(−16)	3.93(−17)	1.21(−16)	2.29(−16)
2.25(+8)	8.24(−17)	1.84(−16)	4.36(−17)	7.88(−17)	1.29(−16)	1.39(−17)	4.27(−17)	8.12(−17)
4.50(+8)	2.91(−17)	6.51(−17)	1.54(−17)	2.79(−17)	4.57(−17)	4.92(−18)	1.51(−17)	2.87(−17)

function of electron temperature with the experimental plasma Maxwellian rate coefficients of Müller (1999) who deduced his rate coefficients from the recombination measurements by Linkemann et al. (1995). We also compare our results with those of the recent calculations of Gu (2004), who used a fully-relativistic factorized distorted-wave approximation.

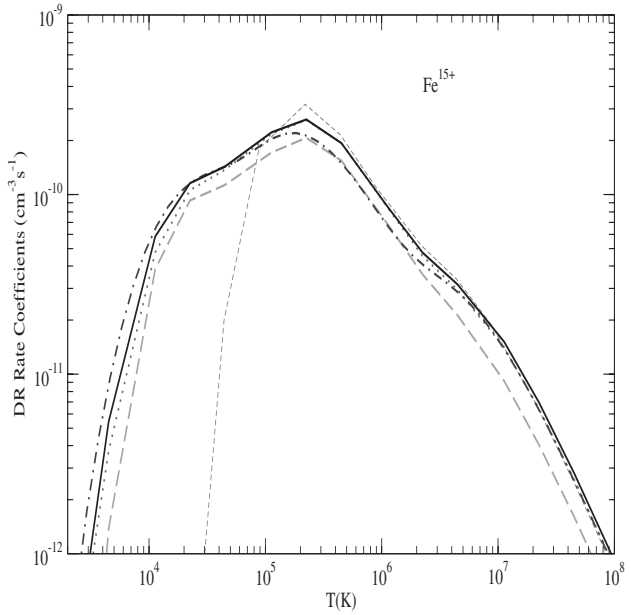

Fig. 4. Total dielectronic recombination rate coefficients for Fe^{15+}, as a function of electron temperature (in Kelvin). The solid curve represents our intermediate coupling MCBP results. The experimental results of Müller (1999) determined from the measurements of Linkemann et al. (1995) are represented by dotted-dashed line. The dotted line (lying just on top of the solid curve) represents the recent fully-relativistic results of Gu (2004). The fitting data of Mazzotta et al. (1998), based on the work of LaGattuta & Hahn (1984), is represented by the short dashed line. Our *LS* -coupling configuration-mixed results are represented by the long-dashed line.

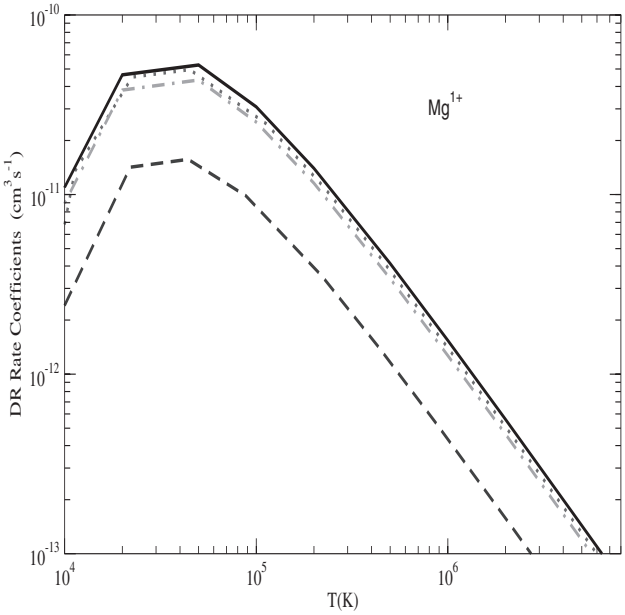

Fig. 5. Total dielectronic recombination rate coefficients for Mg^{+} as a function of electron temperature (in Kelvin). The solid curve represents our intermediate coupling MCBP results. The dotted line (lying just below the solid curve) represents the recent fully-relativistic results of Gu (2004). Our *LS* -coupling results are represented by dashed-dot curve. The lowest (dashed) curve represents the fitting data of Mazzotta et al. (1998), based on the work of LaGattuta & Hahn (1984).

As it can be seen, both our calculations and those of Gu (2004) agree very well with the experimental rate coefficients. Our *LS* -coupling results are also shown. Our *LS* -coupling results agree quite well in shape and magnitude with our intermediate coupling MCBP results, except at low temperatures where the results are sensitive to the exact position of near-threshold resonances. The data provided for Fe^{15+} by Mazzotta et al. (1998) is based on the high temperature ($\gtrsim 3 \times 10^6$ K) results of LaGattuta & Hahn (1984), extended to lower temperatures following Mattioli (1988), and is in good agreement with that presented by Arnaud & Raymond (1992), which is based on the results of Jacobs et al. (1977). However, these results (Mazzotta et al. 1998) only agree with both our results and those of Gu (2004) above 10^5 K. The drop-off at lower temperatures indicates that none of the historical works treated near-threshold resonances adequately. Finally, the contributions from $2p \rightarrow 3l$ core excitations to DR for Fe^{15+} become significant above 10^6 K and this is clearly seen from the shoulder -like structure in the figure.

Figure 5 compares our MCBP intermediate coupling total dielectronic recombination rate coefficients for Mg^{+} with those from both the recent calculations of Gu (2004) and the results obtained from the fitting data provided by Mazzotta et al. (1998), based on the work of LaGattuta & Hahn (1984). The agreement between our *LS* - and intermediate coupling MCBP results and those of the recent calculations of Gu (2004) is excellent. *LS* -coupling results are still used in modelling of light elements in fusion research and this is another reason why we present them along with the intermediate coupling MCBP results. It can be seen also that the overall shape of the curve representing the results of LaGattuta & Hahn (1984), upon which the fitting data of Mazzotta et al. (1988) is based, lie about a factor of 3 lower.

Figure 6 shows the present *LS* - and intermediate coupling total dielectronic recombination rate coefficients as a function of temperature for Ca^{9+}. The agreement between our results and those of Gu (2004) are near perfect over the full range of electron temperatures. Results of the fitting data of Mazzotta et al. (1998), based on the work of Jacobs et al. (1980), agree with the latest theoretical results only above 10^5 K.

In Fig. 7 we compare our MCBP intermediate coupling total dielectronic recombination rate coefficients for Zn^{19+} with those of Gu (2004). Excellent agreement is obtained between the results of these two calculations. Although our *LS* -coupling results include the mass-velocity and Darwin corrections the disagreement with our MCBP results is clearly seen at low temperatures. This indicates the importance of spin-orbit energy splittings for near threshold resonances as Z increases.

Figure 8 shows our multi configuration *LS* - and intermediate coupling total dielectronic recombination rate coefficients for Mo^{31+}. Here the difference in the totals is governed by the presence or absence of near-threshold resonances. The differences between *LS* and intermediate coupling results at low temperatures, as can be clearly seen in Figs. 7 and 8, may be explained as follows: at high charge the level splitting is large but LS calculations use a term energy that is a weighted level

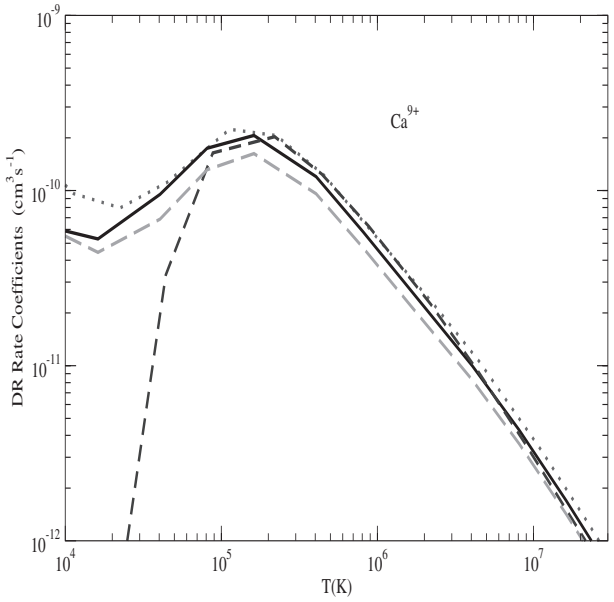

Fig. 6. Total dielectronic recombination rate coefficients for Ca^{9+} as a function of electron temperature (in Kelvin). We compare our *LS*- and intermediate coupling MCBP results with the data adopted by Mazzotta et al. (1998) and those of Gu (2004). The solid curve represents our intermediate coupling MCBP results. The dotted line (lying just on top of the solid curve) represents the recent fully-relativistic results of Gu (2004). The fitting data of Mazzotta et al. (1998), based on the work of Jacobs et al. (1980), is represented by the short-dashed line. Our *LS*-coupling results are represented by the long-dashed line.

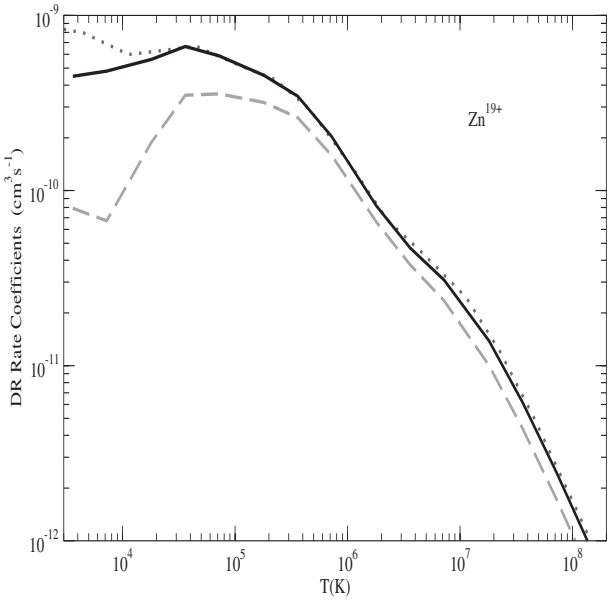

Fig. 7. Total dielectronic recombination rate coefficients for Zn^{19+} as a function of electron temperature (in Kelvin). Our *LS*- and MCBP intermediate coupling results are compared with those of Gu (2004). The dotted line (lying just on top of the solid curve) represents the recent fully-relativistic results of Gu (2004). Our *LS*-coupling results are represented by the long-dashed line.

average (of the observed). Consequently, low energy resonances (associated with $\Delta n = 0$ DR) have significantly different energies between LS and IC calculations and this shows up at low-T via the Maxwellian exponential factor.

5. Summary

We have carried out systematic calculations of dielectronic recombination data for the sodium-like isoelectronic sequence as part of an assembly of a dielectronic recombination database necessary for the modelling of dynamic finite-density plasmas (Badnell et al. 2003). Calculations were carried out in a multi-configuration intermediate coupling Breit-Pauli approximation for all ions for Mg^{+} to Zn^{19+}, as well as Kr^{25+}, Mo^{31+} and Xe^{43+} using non-relativistic (up to Zn) and semi-relativistic (from Zn) radial functions.

The good agreement between our intermediate coupling MCBP results and the measurements on Fe^{15+} (Likemann et al. 1995) and Ni^{17+} (Fogle et al. 2003b) is a good benchmark for the approximations used in obtaining the results presented in this paper, particularly for the higher charged ions. At lower charges, the agreement with the theoretical results of Gu (2004) leads us to believe that the results of these most recent calculations have converged sufficiently for the needs of diagnostic plasma modelling.

To this end, we have calculated *LSJ* final-state level-resolved dielectronic recombination rate coefficients in a form which will be useful for the modellers of both astrophysical and fusion plasmas (available at

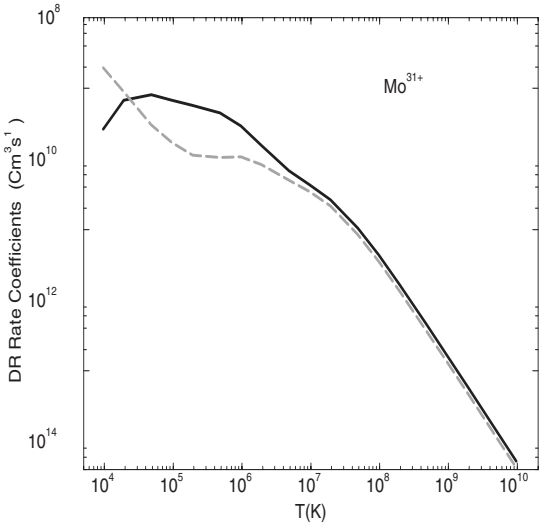

Fig. 8. Total dielectronic recombination rate coefficients for Mo^{31+} as a function of electron temperature (in Kelvin).The solid curve represents our MCBP intermediate coupling results. Our *LS*-coupling results are represented by the long-dashed line.

`http://www-cfadc.phy.ornl.gov/data_and_codes`). Although our approximations are such that each final-state level-resolved dielectronic recombination rate coefficient may not be as highly accurate as some of the most sophisticated techniques available today, we have calculated a consistent set of data over a wide range of electron temperatures and for a large number of atomic ions in order to maximize the available information for modelling work. In order to facilitate the further application of our data, we have presented fits to our MCBP total DR rate coefficients.

We have presented selected initial and final-state-resolved and total rate coefficients for some ions of interest in Figs. 1 to 8 and have made comparisons, where possible, with previous works. We have occasionally found large disagreements with the recommended DR data Mazzotta et al. (1998) for the electron temperatures below $\sim 5 \times 10^5 Z^2$ K, which is important for photoionized plasmas.

Our high-temperature total rate coefficients should be accurate to better than ~30%. The main uncertainty is due to the omission of the effects of external electric and magnetic fields. At low temperatures, typical of photoionized plasmas, the main uncertainty is due to the uncertainty in position of near threshold resonances. In the future we will present dielectronic recombination data for further M-shell isoelectronic sequences, as discussed previously (Badnell et al. 2003).

Acknowledgements. This work was supported in part by the US Department of Energy, Office of Fusion Energy Sciences. Z.A. thanks the Turkish State Planning Organization (DPT) for a local computing grant.

References

Altun, Z., Yumak, A., Badnell, N. R., Colgan, J., & Pindzola, M. S. 2004, A&A, 420, 775
Andersen, L. H., Bolko, J., & Kvistgaard, P. 1990, Phys. Rev. A, 41, 1293
Arnaud, M., & Raymond, J. 1992, ApJ, 398, 394
Arnaud, M., & Rothenflug, R. 1985, A&AS, 60, 425
Badnell, N. R. 1986, J. Phys. B, 19, 3827
Badnell, N. R. 1997, J. Phys. B, 30, 1
Badnell, N. R., Pindzola, M. S., Dickson, W. J., et al. 1993, ApJ, 407, 91, L4441
Badnell, N. R., O'Mullane, M., Summers, H. P., et al. 2003, A&A, 406, 1151
Bartsch, T. , Schippers, S., Müller, A., et al. 1999, Phys. Rev. Lett., 82, 3779
Böhm, S., Schippers, S., Shi, W., et al. 2001, Phys. Rev. A, 64, 032707
Böhm, S., Schippers, S., Shi, W., et al. 2002, Phys. Rev. A, 65, 052728
Burgess, A. 1964, ApJ, 139, 776
Burgess, A. 1965, ApJ, 141, 1588
Burgess, A., & Summers, H. P. 1969, ApJ, 157, 1007
Colgan, J., Pindzola, M. S., Whiteford, A. D., & Badnell, N. R. 2003, A&A, 412, 597
Colgan, J., Pindzola, M. S., & Badnell, N. R. 2004, A&A, 417, 1183
Fogle, M., Eklöw, Lindroth, E., et al. 2003a, J. Phys. B, 36, 2563
Fogle, M., Badnell, N. R., Eklöw, Mohamed, T., & Schuch, R. 2003b, A&A, 409, 781
Griffin, D. C., Pindzola, M. S., & Bottcher, C. 1986, Phys. Rev. A, 33, 3124
Griffin, D. C., & Pindzola, M. S. 1987, Phys. Rev. A, 35, 2821
Griffin, D. C., Pindzola, M. S., & Krylstedt, P. 1989, Phys. Rev. A, 40, 6699
Griffin, D. C. Robicheaux, F., & Pindzola, M. S. 1998, Phys. Rev. A, 57, 2708
Gwinner, G., Hoffknecht, A., Bartsch, T., et al. 2000, Phys. Rev. Lett., 84, 4822
Gu, M. F., 2004, ApJS, 153, 389
Jacobs, V. L., Davis, J., & Kepple, P. C. 1976, Phys. Rev. Lett., 37, 1390
Jacobs, V. L., Davis, J., Kepple, P. C., & Blaha, M. 1977, ApJ, 211, 605
Jacobs, V. L., Davis, J., Rogerson, J. E., et al. 1980, ApJ, 239, 1119
Kraemer, S. B., Ferland, G. J., & Gabel, J. R. 2004, ApJ, 604, 556
LaGattuta, K. J., & Hahn, Y. 1984, Phys. Rev. A, 30, 316
Linkemann, J., Kenntner, A., Müller, A., et al. 1995 Nucl. Instrum. Methods Phys. Res. Sect. B, 98, 154
Mattioli, M. 1988, Euratom-CEA Report No. EUR-CEA-FC-1346
Mazzotta, P., Mazzitelli, G., Colafrancesco, S., & Vittorio, N. 1998, A&AS, 133, 403
Mitnik, D. M., Pindzola, M. S., & Badnell, N. R. 1999, Phys. Rev. A, 59, 3592
Mitnik, D. M., & Badnell, N. R. 2004, A&A, 425, 1153
Netzer, H. 2004, ApJ, 604, 551
Nussbaumer, H., & Storey, P. J. 1983, A&A, 126, 75
Müller, A. 1999, Int. J. Mass Spectrom., 192, 9
Pindzola, M. S., Badnell, N. R., & Griffin, D. C. 1992, Phys. Rev. A, 46, 5725
Robicheaux, F., & Pindzola, M. S. 1997, Phys. Rev. Lett., 79, 2237
Robicheaux, F., Pindzola, M. S., & Griffin, D. C. 1998, Phys. Rev. Lett., 80, 1402
Savin, D. W., & Laming, J. M. 2002, ApJ, 566, 1166
Shull, J. M., & van Steenberg, M. 1982, ApJS, 48, 95
Schippers, S., Bartsch, T., Brandau, C., et al. 2000, Phys. Rev. A, 62, 022708
Summers, H. P. 2003, ADAS User Manual (v2.6), `http://adas.phys.strath.ac.uk/adas/docs/manual`
Zatsarinny, O., Gorczyca, T. W., Korista, K. T., Badnell, N. R., & Savin, D. W. 2003, A&A, 412, 587
Zatsarinny, O., Gorczyca, T. W., Korista, K. T., Badnell, N. R., & Savin, D. W. 2004a, A&A, 417, 1173
Zatsarinny, O., Gorczyca, T. W., Korista, K. T., Badnell, N. R., & Savin, D. W. 2004b, A&A, 426, 699